EBioMedicine 47 (2019) 221–234

Contents lists available at ScienceDirect

EBioMedicine

journal homepage: www.ebiomedicine.com

EBioMedicine
Published by THE LANCET

Research paper

Dual lysosomal-mitochondrial targeting by antihistamines to eradicate leukaemic cells

Josep M. Cornet-Masana [a,b,c], Antònia Banús-Mulet [a,d], José M. Carbó [a], Miguel Ángel Torrente [c,e], Francesca Guijarro [c,e,f], Laia Cuesta-Casanovas [a,g], Jordi Esteve [a,c,e,f], Ruth M. Risueño [a,*]

[a] Josep Carreras Leukaemia Research Institute (IJC). Barcelona, Spain
[b] Institut d'Investigació en Ciències de la Salut Germans Trias i Pujol (IGTP). Badalona, Spain
[c] Faculty of Medicine, University of Barcelona, Spain
[d] Faculty of Pharmacy, University of Barcelona, Spain
[e] Department of Haematology, Hospital Clínic, Barcelona, Spain
[f] Institut d'Investigacions Biomèdiques August Pi i Sunyer (IDIBAPS), Barcelona, Spain
[g] Faculty of Biosciences, Autonomous University of Barcelona, Spain

ARTICLE INFO

Article history:
Received 18 July 2019
Received in revised form 8 August 2019
Accepted 9 August 2019
Available online 28 August 2019

Keywords:
Leukaemia
Antihistamines
Ebastine
Lysosomes
Mitochondria

ABSTRACT

Background: Despite great efforts to identify druggable molecular targets for AML, there remains an unmet need for more effective therapies.
Methods: An *in silico* screening was performed using Connectivity Maps to identify FDA-approved drugs that may revert an early leukaemic transformation gene signature. Hit compounds were validated in AML cell lines. Cytotoxic effects were assessed both in primary AML patient samples and healthy donor blood cells. Xenotransplantation assays were undertaken to determine the effect on engraftment of hit compounds. The mechanism of action responsible for the antileukaemic effect was studied focussing on lysosomes and mitochondria.
Findings: We identified a group of antihistamines (termed ANHAs) with distinct physicochemical properties associated with their cationic-amphiphilic nature, that selectively killed leukaemic cells. ANHAs behaved as antileukaemic agents against primary AML samples *ex vivo*, sparing healthy cells. Moreover, ANHAs severely impaired the *in vivo* leukaemia regeneration capacity. ANHAs' cytotoxicity relied on simultaneous mitochondrial and lysosomal disruption and induction of autophagy and apoptosis. The pharmacological effect was exerted based on their physicochemical properties that permitted the passive targeting of both organelles, without the involvement of active molecular recognition.
Interpretation: Dual targeting of lysosomes and mitochondria constitutes a new promising therapeutic approach for leukaemia treatment, supporting the further clinical development.
Fund: This work was funded by the Fundación Mutua Madrileña (RMR), CaixaImpulse (RMR), the Spanish Ministry of Economy (RMR), the Josep Carreras International Leukaemia Foundation (RMR), l'Obra Social "La Caixa" (RMR), and Generalitat de Catalunya (IJC).

1. Introduction

Acute myeloid leukaemia (AML) is a clinically and biologically heterogeneous disease characterized by the accumulation of immature transformed myeloid progenitors in bone marrow (BM). Although significant research efforts have been invested in improving outcomes for AML patients, the standard therapy for most subtypes of newly diagnosed AML has remained practically unchanged over the past 4 decades, and the prognosis is still poor [1]. Indeed, most patients with AML will relapse after achieving complete remission, with treatment of refractory and relapsed AML being challenging in clinics. Therefore, new therapeutic approaches with high specificity and effectiveness are urgently needed.

Abbreviations: 3-MA, 3-methyladenine; ALL, Acute lymphoblastic leukaemia; ANHA, AntiNeoplastic HRH1 inverse Agonist; AML, Acute Myeloid Leukaemia; BM, Bone Marrow; CAD, Cationic Amphiphilic Drug; CFU, Colony-forming Unit; CML, Chronic Myeloid Leukaemia; CMML, Chronic Myelomonocytic Leukaemia; EC50, Effective concentration 50; hERG, Potassium voltage-gated channel subfamily H member 2; HR, Histamine Receptor; LGALS1, Galectin-1; LMP, Lysosomal Membrane Permeabilization; LSC, Leukemic Stem Cell; mAChR, Muscarinic AcetylCholine Receptor; NAC, *N*-acetylcysteine; NSG, NOD.Cg-Prkdcscid Il2rgtm1Wjl/SzJ; ROS, Reactive Oxygen Species; TPSA, Topological Polar Surface Area; UCB, Umbilical Cord Blood.

* Corresponding author at: Josep Carreras Leukaemia Research Institute, Campus ICO-GTP, Crta Can Ruti. Camí de les Escoles, s/n, 08916 Badalona Barcelona, Spain.
E-mail address: risueno@carrerasresearch.org (R.M. Risueño).

https://doi.org/10.1016/j.ebiom.2019.08.021

Research in context

Evidence before this study

Despite great efforts to identify druggable molecular targets for acute myeloid leukaemia, there remains an unmet need for more effective therapies. In this quest, *in silico* identification of repurposing drug candidates has been proven useful in the search for potential therapies. As such, several antihistamines have been preclinically described as antineoplastic agents in non-AML tumors.

Added value of this study

In our study, we described the antileukaemic potential of several antihistamines and demonstrated its histamine receptor-independence. Rather than a specific molecular target recognition, the mechanism of action was found to rely on the simultaneous disruption of lysosomes and mitochondria, based on the physicochemical properties of these drugs.

Implications of all the available evidence

The preclinical results presented in the study are in line with previous results in lung cancer and constitute a stepping stone towards the development of novel treatments for AML independent of active molecular recognition and based on simultaneous lysosomal and mitochondrial functionality disruption.

AML displays a high degree of heterogeneity that evolves through disease progression and/or relapse, affecting both the genotype and the phenotype of leukaemic subclones [2–6]. Cytogenetically, 50% of AML patients present normal karyotypes, suggesting the existence of other molecular events in leukaemogenesis [7]. Despite this disease complexity, MLL fusion genes have been demonstrated capable of initiating human leukaemogenesis *in vivo*, as their expression is sufficient to transform human haematopoietic progenitors and mature cells into leukaemic cells [8–10]. Specifically, MLL-AF9 fusion protein does not require collaborating mutations to induce leukaemia transformation [11]. Although MLL-AF9 rearrangement is rarely found in AML patients (below 1%) [12,13], MLL-AF9 AML model faithfully recapitulates key aspects for this disease, including *in vivo* regeneration capacity, clonogenicity and phenotype [8,9].

Although the hypothesis that histamine might be involved in carcinogenesis was proposed several decades ago [14], it remains under discussion today. Indeed, the evidence linking antihistamines *per se* to cancer is controversial and complex [15,16]. In the Haematology field, the antileukaemia effect of terfenadine has been recently described, suggesting a non-canonical mechanism of action [17]. Similar results were obtained in other solid tumors when different antihistamines were studied for their antineoplastic activity [18–24], mainly through an HRH1-independent mechanism.

Based on the gene expression profile associated with MLL-AF9-driven early transformation events in AML, a group of antihistamines was identified as potent antileukaemic agents due to their histamine receptor-independent physicochemical properties allowing mitochondrial and lysosomal disruption. Simultaneously targeting both organelles constitutes a new therapeutic approach for haematological neoplasias, affecting both the bulk population and the most primitive cell fraction without significant effect on their healthy counterparts.

2. Materials and methods

2.1. AML cell lines and cell cultures

Cell lines HL-60 (ACC-3), KG-1 (ACC-14), MonoMac-1 (ACC-252) K-562 (ACC-10), Jurkat (ACC-282), RPMI-8402 (ACC-290), CCRF-CEM (ACC-240), RAMOS (ACC-603), GRANTA-519 (ACC-342), RPMI-8226 (ACC-402), JJN-3 (ACC-541) and U-266 (ACC-9) were obtained from DSMZ (Braunschweig, Germany). THP-1 cell line (TIB-202™) was obtained from ATCC (Manassas, VA, USA). HBL-2 cell line was kindly supplied by Dr. Pérez-Galán.

2.2. Primary samples

Primary AML samples were obtained from patients diagnosed at Hospital Clínic of Barcelona (Spain) and Hospital Germans Trias i Pujol (Badalona, Spain). AML diagnosis and classification were based on standard WHO criteria (70). Main AML patient's characteristics are summarized in Table S1. Mononuclear cells (MNCs) were isolated by Ficoll density gradient centrifugation (GE, Chicago, IL, USA). All patients provided written informed consent in accordance with the Declaration of Helsinki, and the study was approved by the corresponding Ethics Committees. Blood mature MNCs were isolated from healthy-donor buffy coats provided by Banc de Sang i Teixits (BSiT, Barcelona, Spain). Umbilical cord blood was provided by BSiT, and MNCs were depleted for lineage marker-positive cells using magnetic separation with human Lineage Cell Depletion kit (Miltenyi Biotec, Bergisch Gladbach, Germany) following manufacturer's recommendations.

2.3. Drugs and antibodies

All drugs were resuspended in H_2O (Thermo Fischer Scientific, Waltham, MA, USA), DMSO (Sigma-Aldrich, St. Louis, MO, USA) or ethanol (VWR) according to manufacturer's specifications. Antibodies used in this study are summarized in Table S3.

2.4. Cytotoxicity assays

2×10^5 (72 h assays), 3×10^5 (48 h assays) or 7.5×10^5 (primary AML) cells per mL were cultured in 96-well plates and all drugs were added at the indicated concentrations. In co-culture experiments, 2×10^5 CFSE-stained HS-5 cells per mL were seeded in 96-well plates. AML cell lines at 2×10^5 cells per mL were subsequently added. In *Z*-VAD-FMK experiments cells were pretreated 20 min with Z-VAD-FMK 50 μM. In α-tocopherol experiments, cells were pretreated for 24 h with growing concentrations of α-tocopherol and later incubated with antihistamines for 48 h. Cell viability was measured by 7-AAD (eBioscience, San Diego, CA, USA) exclusion and Hoechst33342 (Sigma-Aldrich) positivity staining by flow cytometry, and cell count was obtained by volume. In experiments with primary cells, analyses were performed inside the blast population as detected by blast gates ($CD45^{low}$ SSC^{int}).

2.5. Proliferation assay

HL-60 and KG-1 cells were stained with 2,5 μM CFSE (CellTrace™ CFSE Cell Proliferation kit, Thermo Fisher). Drugs were added at the indicated concentrations.

2.6. Clonogenicity assay

1×10^3 cells of AML cell lines or 50×10^3 primary AML cells or lin-depleted UCB cells were treated at the indicated concentration for 18 h and cultured in 1 mL of MethoCult H4034 Optimum (StemCell Technologies, Vancouver, BC, Canada). Colonies were screened based

on morphology and cellularity at day 7 (cell lines) or 14 (AML primary cells and lineage-depleted UCB cells).

2.7. In vivo studies

6–8 week-old NOD.Cg-Prkdcscid Il2rgtm1Wjl/SzJ (NSG, Jackson Laboratories) mice were myeloablated with busulfan (30 mg/kg IP) at day 0. CD3-depleted primary AML patient samples or lineage-depleted UCB cells were *ex vivo* treated in the indicated conditions, and 4–34 $\times 10^6$ (AML) or 12–14 $\times 10^4$ (lin^- UCB) cells were injected IV and left 8–10 weeks untreated. Engraftment was determined as the percentage of live human CD45-expressing cells in bone marrow as assessed by flow cytometry. Mice were randomized and blind-coded at the beginning of the experiment.

2.8. HRH1 immunofluorescence

A total of 3×10^5 cells were attached to poly-L-lysine (50 μg/mL)-coated coverslips and fixed with formaldehyde 4% (Sigma), blocked with γ-globulin (10 μg/mL) and stained with Hoechst33342 and HRH1 antibody (Antibodies-online GmbH, Aachen, Germany). Samples were observed in a Leica DMI6000 B fluorescence microscope (Leica, Wetzlar, Germany) and the images were analysed with Image J.

2.9. Lysotracker

4×10^5 cells per mL were treated, washed in HBSS and incubated with 50 nM Lysotracker DeepRed (Thermo Fisher) and Hoechst33342 for 30 min at 37 °C. Cells were washed twice with HBSS and acquired in a flow cytometer. For the microscopic analysis, 2×10^5 cells per condition were treated, washed with complete medium and incubated 1 h with 100 nM LysoTracker DeepRed and Hoechst 33342 at 37 °C. Cells were attached to chambered coverslips (μ-Slide 8 well, Ibidi) previously treated with Poly-L-Lysine 50 μg/mL. Live cell images were acquired with a Zeiss LSM880 confocal microscope (Zeiss, Jena, Germany).

2.10. Lysosomal membrane permeabilization

3×10^5 cells previously treated for 18 or 48 h with selected drugs were attached to poly-L-lysine (50 μg/mL)-coated coverslips, fixed with formaldehyde 4% (cathepsin B) or cold methanol (galectin-1) and permeabilized with Triton X100 0.2%. Cells were then blocked with γ-globulin (10 μg/mL) and incubated with cathepsin B (NBP1–86048, 1:100) or galectin-1 (ab25138, 1:1000) antibodies. Cells were subsequently incubated with Hoechst33342 and Alexa Fluor 488 Goat Anti-Rabbit IgG. Images were acquired in a confocal microscope Zeiss LSM880 and analysed with Fiji software [25].

2.11. Cyto-ID staining

4×10^5 cells per mL were treated for 18 h with drugs at the indicated concentrations, washed in PBS and incubated 30 min at 37 °C in PBS with 5% FBS containing Hoechst 33342, 7-AAD and Cyto-ID green fluorescent dye (CYTO-ID ® Autophagy detection kit, Enzo Life Sciences, Farmingdale, NY, USA) at a 1:4000 dilution. Cells were washed with PBS and acquired in a flow cytometer.

2.12. LC3B immunoblotting

10×10^6 AML cell lines or $25–50 \times 10^6$ primary AML cells per condition were treated in indicated conditions and subsequently harvested and lysed in RIPA lysis buffer. Antibodies used for this technique are listed on supplementary table 2. Images were acquired in a LICOR Odyssey Imager and quantified using Fiji software.

2.13. Mitochondrial reactive oxygen species (ROS)

4×10^5 cells/ml were treated at the indicated concentration of drugs for 6 h and subsequently incubated with mitochondrial ROS detector *MitoSOX Red Mitochondrial Superoxide Indicator* (Thermo Fischer Scientific) 5 μM and Hoechst33342 for 10 min at 37 °C. Cells were washed twice with HBSS and acquired in a FACSCantoII cytometer.

2.14. Rhodamine 123 assay

Changes in mitochondrial membrane potential were assessed using the rhodamine 123 dye. Briefly, cells were treated for 18 h, washed with PBS and incubated with rhodamine-123 50 nM (15 min, 37 °C). Cells were then washed twice with PBS and acquired in a flow cytometer.

2.15. CaspaseGlo assay

4×10^5 cells per mL were seeded in 96-well plates and treated in indicated conditions (50 μL final volume). 50 μL reconstituted CaspaseGlo® 3/7 Assay substrate (Promega) were added, and the mix was incubated 30′ at room temperature. Luminescence was analysed using a Synergy HT Multi-Detection Microplate Reader (BioTek, Winooski, VT, USA) following manufacturer's recommendations.

2.16. Annexin V staining

3×10^5 cells per mL were treated for 48 h with compounds at the indicated concentrations. Annexin V membrane translocation was measured using the Annexin V apoptosis detection kit (Becton Dickinson, Franklin Lakes, NJ, USA) according to the manufacturer's instructions. Data were collected by flow cytometry

2.17. Flow cytometry

All flow cytometric experiments were performed with a FACSCanto II cytometer (Becton Dickinson). All flow cytometric analysis was done using FlowJo software (TriStar, Scottsdale, AZ, USA).

2.18. Statistics

Statistical significance was determined using GraphPad Prism® 6.01 (GraphPad software, La Jolla, CA, USA) by using the statistical tests specified in figure legends. Error bars correspond to SEM. All experiments were done at least 2 times in biological triplicates, unless otherwise specified in the figure legend.

2.19. Ethics approval

All patients provided written informed consent in accordance with the Declaration of Helsinki, and the study was approved by the corresponding Ethics Committees (Ethics Committee Hospital Clínic de Barcelona, Ethics Committee Hospital Germans Trias i Pujol). All experiments involving mice were approved by the Catalan Ethical Committee of Animal Experimentation (CCEEA).

2.20. Availability of data and materials

The datasets used and/or analysed during the current study are available from the corresponding author on reasonable request.

3. Results

3.1. A group of antihistamines displayed antileukaemic effects

To search for drugs that may revert early leukaemogenesis-related events, the MLL-AF9-induced AML model was chosen, as MLL-AF9 not

only is capable of transforming human progenitor blood cells into AML, but also induces the aberrant expression of stem-cell genes that characterize leukaemic stem cells capable of initiating, maintaining and propagating the leukaemia [26]. The gene expression profile induced upon MLL-AF9 expression in CD34+ cord blood cells [27] was screened in the Connectivity Map database [28] in order to search for small bioactive molecules that may revert the transformation-associated gene signature. Unexpectedly, four antihistamines were found among hit compounds (Fig. S1). A primary screening on AML cell lines was performed to validate the results obtained from the *in silico* prediction. AML cell viability remained unaffected in the presence of histamine (natural HR agonist), and HR type 2 (HRH2), HR type 3 (HRH3) and HR type 4 (HRH4) antagonists. However, a subgroup of HRH1 inverse agonists (loratadine, rupatadine, terfenadine and ebastine) (ANHA: AntiNeoplastic HRH1 inverse Agonist) significantly decreased leukaemic survival (Fig. 1A and S2A; Table S4). Indeed, the antileukaemic effect measured by the EC50 on AML cell lines was in the low micromolar range (Fig. 1B and S2B), being similar in MLL-AF9-positive (MonoMac-1, THP-1) and in MLL-AF9-negative (HL-60, KG-1) cell lines (Fig. S3). At that concentration, ANHAs significantly reduced the proliferation rate of AML cells (Fig. 1C and S2C). Moreover, the AML clonogenic capacity as measured by the colony-formation potential decreased in the presence of ANHAs (Fig. 1D). As the block in differentiation is a hallmark of AML, we interrogated the differentiation status of AML cells treated with ANHAs. Upregulation of both CD11b and CD14 differentiation-associated granulocyte and monocyte surface markers was detected upon treatment (Fig. 1E and S2D). In concordance, treatment with ANHAs lead to a G2/M cell-cycle arrest (Fig. 1F and S2E). Moreover, ANHA treatment synergized with cytarabine, the backbone of chemotherapy regimen in AML (Fig. 1G), enabling the eradication of cytarabine-resistant cells. Due to the well-described BM microenvironment protection on AML [29], the antineoplastic effect of ANHA-drug treatment was interrogated in a more relevant *in vitro* co-culture system with HS-5 human BM stroma cells. Treatment of AML cells in direct contact with HS-5 stromal monolayers did not overcome the cytotoxic effect of ANHAs (Fig. 1H and S2F). Our results suggest that ANHA induced cytotoxicity on AML cells by promoting differentiation and G2/M accumulation, and this neoplastic effect is stroma-independent.

The antileukaemic effect of ANHA was then evaluated *ex vivo* in 16 primary AML patient samples. The reduction of cell viability upon treatment in all AML samples tested was dose- and time-dependent (Fig. 2A). In contrast to AML cell lines (Fig. 1) where a 50% cell death was achieved in the presence of 5–10 μM of each drug at 48 h post-treatment, primary AML samples were more resistant, and a clinically significant cytotoxic effect was detected at day 6. Interestingly, all the AML samples tested were sensitive to the treatment. In order to measure the proliferation and differentiation ability of individual AML cells and, therefore, their *ex vivo* stem-cell properties, the clonogenic capacity was measured 18 h after treatment. Additionally, the total number of colonies decreased to approximately 50% (Fig. 2B), suggesting that ANHAs affected the most primitive fraction of AML cells.

As ANHAs are already FDA- and/or EMA-approved antihistamines, the therapeutic maximal concentration achieved in plasma is already known and ranges between 1 and 200 nM [30]. However, the cytotoxic effect observed on AML cells was achieved at a low microMolar range; therefore, the safety of these treatments on healthy blood cells was tested at the same conditions as previously described for primary AML samples. The cell viability of each blood-cell subtype (T, B and myeloid cells) remained largely unaffected upon treatment; only the myeloid population was significantly reduced in the presence of rupatadine and ebastine at day 6 (Fig. 2C). Remarkably, treatment with ANHAs spared the clonogenic capacity of healthy haematopoietic progenitor/stem cells as shown in Fig. 2D, where no differences were observed in the total number or relative frequency of each type of CFUs. Only terfenadine significantly reduced the total number of CFUs and, also considering its withdrawal from the market due to potential cardiotoxicity, its study as a candidate was discontinued [31]. The ratio between viability reduction and total CFUs generated from healthy blood cells *versus* AML cells was calculated to reveal the higher selectivity of ANHAs for targeting AML (Fig. 2E).

3.2. ANHA treatment selectively impaired the leukaemia regeneration capacity in vivo

Next, the effect of ANHAs on the *in vivo* engraftment potential was evaluated. Primary AML samples were treated *ex vivo* for 18 h and transplanted into adult conditioned immunocompromised NSG mice. Transplanted mice were left untreated for 8–10 weeks in order to measure the leukaemia regeneration capacity of AML cells upon treatment. As shown in Fig. 3A, ebastine severely reduced the leukaemia burden in BM, diminishing the presence of human AML cells in BM by >90%. Indeed, 75% ebastine-treated mice displayed <3% AML blasts in BM as compared to vehicle-treated control. The treatment with rupatadine also induced a reduction of the engraftment capacity of AML cells in >50%. However, no significant differences were detected in the leukaemia regeneration capacity upon loratadine treatment. As healthy control, lineage-depleted umbilical cord blood cells (lin^- UCB cells) were treated similarly to AML cells and transplanted into NSG mice. In concordance with the lack of cytotoxic effect in healthy blood cells demonstrated in Fig. 2, lin^- UCB cells *ex vivo* treated with ebastine displayed a slight reduction in normal haematopoietic potential as measured by the human regeneration capacity on BM (Fig. 3B). Indeed, the frequency of the most primitive haematopoietic human cell fraction represented by $CD34^+$ cells in BM was equivalent in all treated animals as compared to vehicle-treated mice (Fig. 3C). Similar results were obtained in the $CD13^+$ myeloid and $CD19^+$ lymphoid cell population (Fig. 3C). Again, the ratio between the engraftment reduction levels observed in AML *vs.* healthy blood cells revealed the high specificity towards neoplastic cells (Fig. 3D). Thus, treatment with ANHAs dramatically reduced the regeneration potential of AML cells with little effect on normal HSCs.

3.3. ANHA antineoplastic effect was not mediated by HRH1

Since ANHAs are well-known antihistamines that specifically recognize HRH1, the role of this membrane receptor in leukaemogenesis was studied. First, the cell-surface expression of HRH1 was evaluated on AML cell lines. HRH1s were uniformly expressed on all AML cells (Fig. 4A and B). However, the cytotoxic effect observed upon treatment of AML cells with ANHAs was not reverted in the presence of the natural ligand of HRH1, histamine (Figs. 4C and S4A), and no relationship was found between the sensitivity of AML cells and the affinity of antihistamines for HRH1 as measured by the pKi value (Fig. 4D). To further study the relationship between the antileukemic potential and HRH1, we analysed both HRH1 expression and ANHA cytotoxicity in a broader panel of leukemic cell lines. Although all the different leukaemic cell lines tested were sensitive to ANHA treatment, HRH1 expression and cytotoxicity were inconsistent (Figs. 4E-G and Figs. S4B and S4C); equivalent sensitivity to ANHA treatment was found in leukaemic cells with dramatically different levels of HRH1 (0–100%). These results suggested that ANHAs exerted their effect in a HRH1-independent manner; thus, alternative already described targets were explored. Although many HRH1 antagonists also inhibit muscarinic acetylcholine receptors (mAChR) [32–34], no effect on cell viability was detected upon treatment with mAChR antagonists (Fig. S5A) neither acetylcholine reverted the cytotoxicity induced by ANHAs (Fig. S5B). Next, we investigated the role of the potassium voltage-gated channel subfamily H member 2 (hERG, KCHNH2 or Kv11.1) as many antihistamines block this channel [35–37]. Yet, the survival of AML cells remained largely unaffected in the presence of hERG blockers (Fig. S5C). Therefore, the pharmacological effect of ANHAs on AML cells was not exerted by HRH1 inhibition, mAChR modulation or hERG blockage.

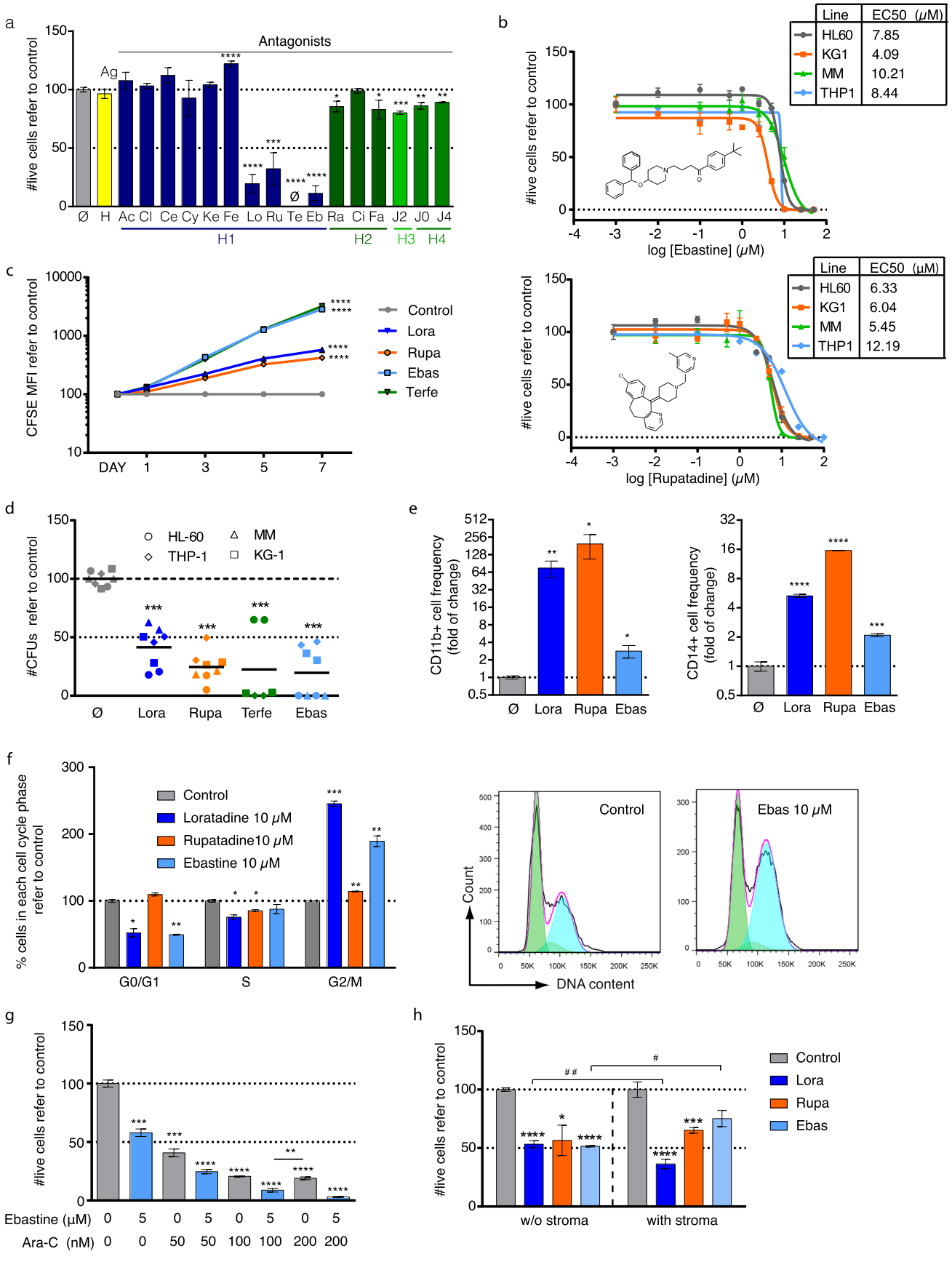
a
#live cells refer to control
Antagonists
Ag
Ø H Ac Cl Ce Cy Ke Fe Lo Ru Te Eb Ra Ci Fa J2 J0 J4
H1 H2 H3 H4
b
Line EC50 (μM)
HL60 7.85
KG1 4.09
MM 10.21
THP1 8.44
log [Ebastine] (μM)
Line EC50 (μM)
HL60 6.33
KG1 6.04
MM 5.45
THP1 12.19
log [Rupatadine] (μM)
c
CFSE MFI refer to control
DAY 1 3 5 7
Control
Lora
Rupa
Ebas
Terfe
d
#CFUs refer to control
HL-60
THP-1
MM
KG-1
Ø Lora Rupa Terfe Ebas
e
CD11b+ cell frequency (fold of change)
CD14+ cell frequency (fold of change)
Ø Lora Rupa Ebas
f
% cells in each cell cycle phase refer to control
Control
Loratadine 10 μM
Rupatadine10 μM
Ebastine 10 μM
G0/G1 S G2/M
Control
Ebas 10 μM
Count
DNA content
g
#live cells refer to control
Ebastine (μM) 0 5 0 5 0 5 0 5
Ara-C (nM) 0 0 50 50 100 100 200 200
h
#live cells refer to control
Control
Lora
Rupa
Ebas
w/o stroma
with stroma

3.4. ANHAs perturbed lysosomes in AML cells

Cationic amphiphilic drugs (CADs) are molecules with a hydrophobic ring structure and a side chain with a cationic amine group [38]. As CADs are not ionized at a physiologic pH and have overall hydrophobicity, they can easily permeate through the plasma membrane [39]. Within the highly acidic lysosomal compartment, the amine is protonated, and the drug is then trapped and concentrated, inducing membrane structure perturbation and compromising cell viability [40,41]. Their uptake is therefore controlled by two major mechanisms: non-specific binding to membrane phospholipids and ion-trapping within acidic cellular compartment [18]. As ANHAs have been described as CADs exerting cytotoxicity effects in solid tumors through lysosomal accumulation [18], the lysosome compartment was examined using the acidotropic probe LysoTracker. As expected for CADs, AML cells treated with ANHAs showed an enlargement of the lysosome mass, as detected by fluorescence microscopy (Fig. 5A and S6A) and flow cytometry (Fig. 5B and S6B); which constitutes a common event preceding the cell death-inducer lysosomal membrane permeabilization (LMP) [42]. This phenomenon was detected by the formation of a punctate pattern of Galectin 1 (LGALS1) (Fig. 5C and S6C), as a result of its translocation from the cytosol to damaged lysosomes. As a consequence of LMP, lysosomal cathepsins are released to the cytoplasm [43], as shown in Fig. 5D and S6D. Likewise, α-tocopherol, a molecule reported to protect lysosomes against CADs based on their redistribution to non-lysosomal membranes and the stabilization of the lysosome membrane itself [44,45], strongly reverted the cytotoxicity induced by ANHAs (Fig. 5E and S7A). In concordance with the increase of the lysosomal compartment upon ANHA treatment, the autophagic flux augmented in the presence of these drugs as measured by CytoID staining by flow cytometry (Fig. 5F and S7B). Indeed, the amount of LC3-II, a canonical marker for autophagic activity [46], was higher in cells treated with ANHAs, both in AML cell lines (Fig. 5G) and primary AML patient samples (Fig. S7C). However, the autophagy inhibitor 3-methyladenine (3-MA) was unable to revert the antileukaemic effect of ANHAs (Fig. 5H and S7D). Thus, ANHAs present lysosomotropism and induce autophagy, although alternative cell death pathways might be involved.

3.5. ANHAs damaged the mitochondrial compartment

Prior to lysosomes, CADs may accumulate in the mitochondrial compartment [47]. Also, LMP can activate the intrinsic apoptosis pathway [48]; consequently, the mitochondrial status was investigated. Mitochondrial oxidative stress measured by the generation of reactive oxygen species (ROS) was induced by ANHAs (Fig. 6A and S8A) and the ROS scavenger *N*-acetylcysteine (NAC) cytoprotected AML cells in their presence (Fig. 6B), in a ROS-dependent manner (Fig. S8B). The mitochondrial membrane potential (ΔΨm) was also severely dissipated upon treatment (Fig. 6C and S8C), suggesting that ANHAs also affected the mitochondrial functionality. Both ROS generation and loss of ΔΨm leads to the activation of the apoptosis-associated executioner caspases 3 and 7. Consequently, caspases 3/7 were activated after ANHA treatment (Fig. 6D and S8D); although the inhibition of caspases by z-VAD-FMK had no significant effect on ANHA treatment induced cell death (Fig. 6E and S8E-F), suggesting that several cell death programs might be activated. Regardless, the canonical apoptosis marker Annexin-V was upregulated in a dose-response manner (Fig. 6F and S8G).

Due to the cross-talk between mitochondrial and lysosomal compartment during activation of the cell death program, the temporal induction of mitochondrial and lysosomal damages was studied. Mitochondrial ROS generation peaked 4 h post-treatment; while caspase 3/7 activation, lysosomal enlargement and autophagosome accumulation were induced 6–12 h after treatment (Fig. 6G). Although ROS is a described LMP-inducer, the increase in lysosomal volume cannot be also attributed, suggesting that ANHAs might be exerting their antileukaemic effect simultaneously on both organelles and are both relevant for cell death.

Lysosomo- and mitochondriotropism require passive membrane diffusion and sequestration inside these organelles. Passive permeability across lipid membranes is correlated positively with lipophilicity and negatively with polarity; thus, high logD (pH 7.4) and low TPSA (topological polar surface area) predicts high passive diffusion across biological membranes [39]. Ion trapping is generally responsible for drug accumulation in lysosomes and mitochondria, where protonation of the amines present in CADs are driven by pH and/or ΔΨ [47]. In concordance with the dual effect on lysosomes and mitochondria, ANHAs had high logD (Fig. 7A) and an intermediate-low TPSA value (Fig. 7B). Indeed, ANHAs clustered when these two parameters were analysed, showing a different profile as compared to non-ANHA antihistamines (Fig. 7B); further confirming the relevance of physicochemical properties rather than specific molecular recognition parameters for their antineoplastic potential (Fig. 7C).

4. Discussion

Despite high complexity and heterogeneity, several alterations in cell organelles are thought to be shared across AML patient cells as compared to their healthy counterparts, including an enlarged lysosomal size and frailty [40,49] and a plethora of mitochondrial changes, such as an increased ROS content [50–53] and dysfunctional metabolism [54], rendering AML cells more vulnerable to drugs targeting those cellular compartments. In an *in silico* screening searching for small molecules that might revert an early transformation signature in AML, several antihistamines were identified as highly-effective and selective antileukaemic agents by a dual mitochondrial-lysosomal targeting. Indeed, this group of antihistamines (ANHAs) were effective against different types of lymphoblastic and myeloid neoplasias, highlighting the potential clinical utility of mitochondrial-lysosomal disrupters for the treatment of leukaemia.

As the transformation process leads, in general, to an increase in the lysosome biogenesis and mass, an alteration in the sphingolipid metabolism, and an augmentation of ROS [55,56], these antihistamines acted also against different types of leukaemia. Mitochondria can be

Fig. 1. A subgroup of antihistamines displays antileukaemic effects in AML cell lines. (A) Viability of KG-1 cells after 72 h-treatment with histamine-related ligands (10 μM). Agonist: histamine (H, yellow). HRH1 antagonists (blue): acrivastine (Ac), clemastine (Cl), cetirizine (Ce), cyproheptadine (Cy), ketotifen (Ke), fexofenadine (Fe), loratadine (Lo), rupatadine (Ru), terfenadine (Te), ebastine (Eb). HRH2 antagonists (dark green): ranitidine (Ra), cimetidine (Ci), famotidine (Fa). HRH3 antagonists (light green): JNJ5207852 (J2). HRH4 antagonists (green): JNJ7777120 (J0), JNJ10191584 (J4). Bars show mean ± SEM of triplicates (2 experiments). (B) Cytotoxicity dose-response curves of HL60 (grey), KG1 (orange), MM (green) and THP1 (blue) cells treated 48 h with ebastine or rupatadine. (C). CFSE proliferation assay in KG1 cells treated with loratadine 10 μM, rupatadine 10 μM, ebastine 10 μM or terfenadine 10 μM. CFSE MFI at days 1, 3, 5 and 7. (D). Clonogenicity assays in AML cell lines treated with loratadine 10 μM, rupatadine 10 μM, terfenadine 10 μM or ebastine 10 μM. CFUs counted at day 10. (E). Expression of monocytic (CD14) and granulocytic (CD11b) markers in KG1 cells treated with 10 μM loratadine, 10 μM rupatadine or 5 μM ebastine for 72 h. Bars show mean ± SEM of triplicates (2 experiments). (F). Cell cycle analysis of KG1 cells treated with loratadine 10 μM, rupatadine 10 μM, or ebastine 10 μM. Left: Frequencies of cell cycle phases referred to control. Bars show mean ± SEM of triplicates (2 experiments). Right: representative cytometric histograms (left: vehicle-treated, right: ebastine-treated; green: G0/G1, yellow: S, blue: G2/M). (G) Viability of KG1 cells treated for 48 h with loratadine 10 μM, rupatadine 10 μM, or ebastine 5 μM in the presence (right) or absence (left) of bone marrow stroma (HS-5). Bars show mean ± SEM of triplicates (3 experiments). (H). 48 h-viability of KG-1 cells treated with ebastine and/or ara-C at the indicated concentration. Bars show mean ± SEM of triplicates of representative experiment (3 experiments). *or# $p < .05$; **or## $p < .01$; *** $p < .001$; **** $p < .0001$ (*t*-tests).

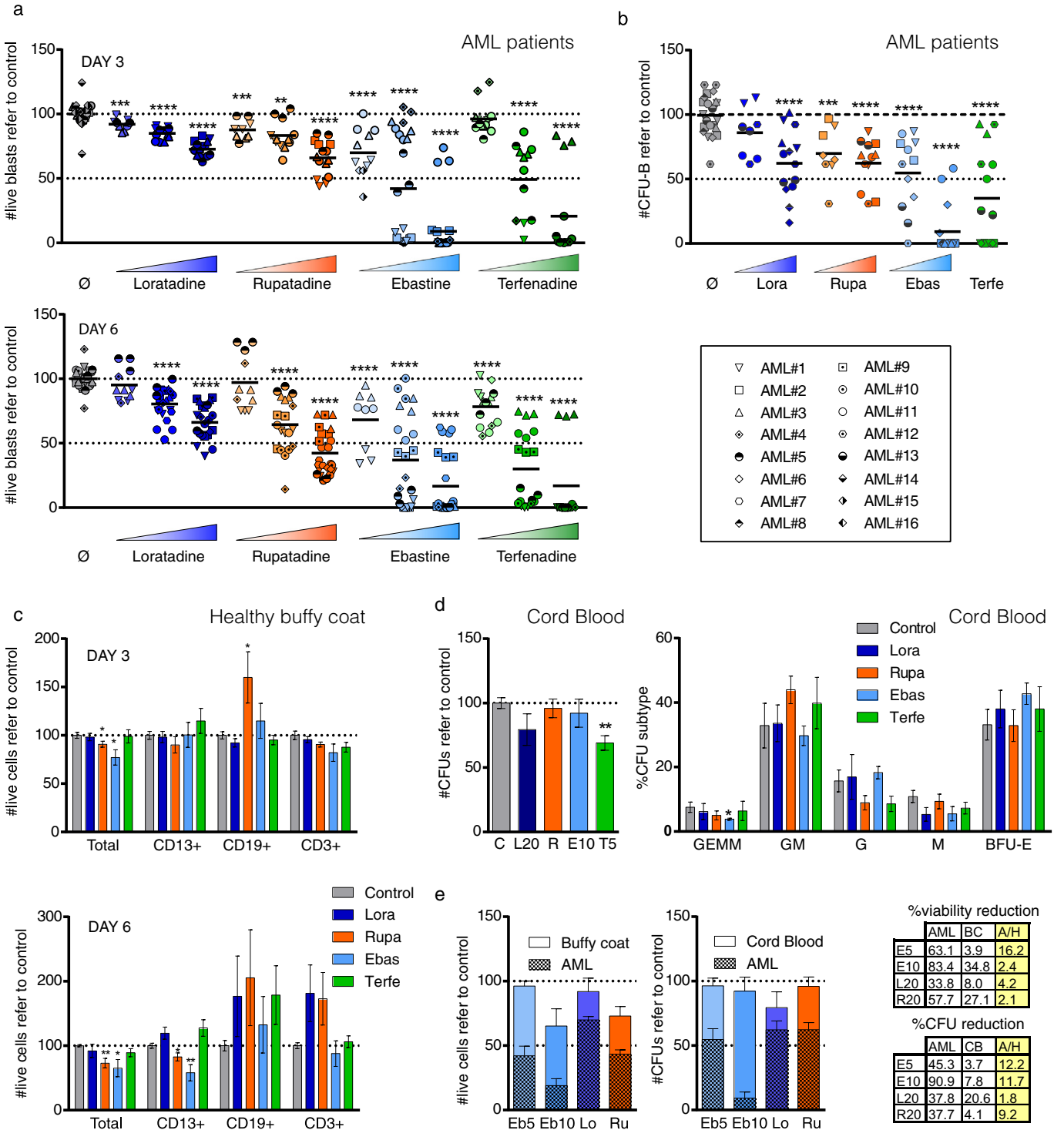

%viability reduction

	AML	BC	A/H
E5	63.1	3.9	16.2
E10	83.4	34.8	2.4
L20	33.8	8.0	4.2
R20	57.7	27.1	2.1

%CFU reduction

	AML	CB	A/H
E5	45.3	3.7	12.2
E10	90.9	7.8	11.7
L20	37.8	20.6	1.8
R20	37.7	4.1	9.2

Fig. 2. ANHAs selectively target AML cells *ex vivo*. (A) AML patient samples were treated with ANHAs loratadine (dark blue; 5, 10 and 20 μM), rupatadine (orange; 5, 10 and 20 μM), ebastine (light blue; 1, 5 and 10 μM) or terfenadine (green; 1, 5 and 10 μM). Blast viability was assessed at day 3 and 6. Each symbol corresponds to an AML patient sample ($n = 16$), and each point to a measure. (B). Clonogenicity assay (day 14) in AML patient samples treated with loratadine 10 and 20 μM (Lora), rupatadine 10 and 20 μM (Rupa), ebastine 5 and 10 μM (Ebas) or terfenadine 5 μM (Terfe). Each symbol corresponds to an AML represents a sample ($n = 8$), each point to a measure. (C). Viability of mononuclear cells from healthy-donor buffy coats was assessed after 3- or 6-day treatment with loratadine 20 μM, rupatadine 20 μM, ebastine 10 μM or terfenadine 5 μM. Bars show mean ± SEM of 5 healthy samples assayed in triplicates. (D). Lineage-depleted UCB cells were applied for 18 h the same treatment as in (C) and cultured as in (B). Left panel: total number of CFUs normalized to control; right panel: frequency of colony subtypes. 3 different samples are represented in triplicates. Bars show mean ± SEM. (E). *Ex vivo* effects of ANHAs on healthy and AML samples were compared in terms of viability (left), and clonogenicity (right). Data represent viability or clonogenicity reduction of treatments with ebastine 5 and 10 μM (Eb), loratadine 20 μM (Lo) or rupatadine 20 μM (Ru). Bars show superimposed mean + SEM of data from Figs. 2A to 2D. Tables show mean percent reduction in viability or CFU formation, as well as its fold of change (FC; effect on AML/ healthy samples). *p < .05; ** p < .01; *** p < .001; **** p < .0001 (Mann-Whitney tests).

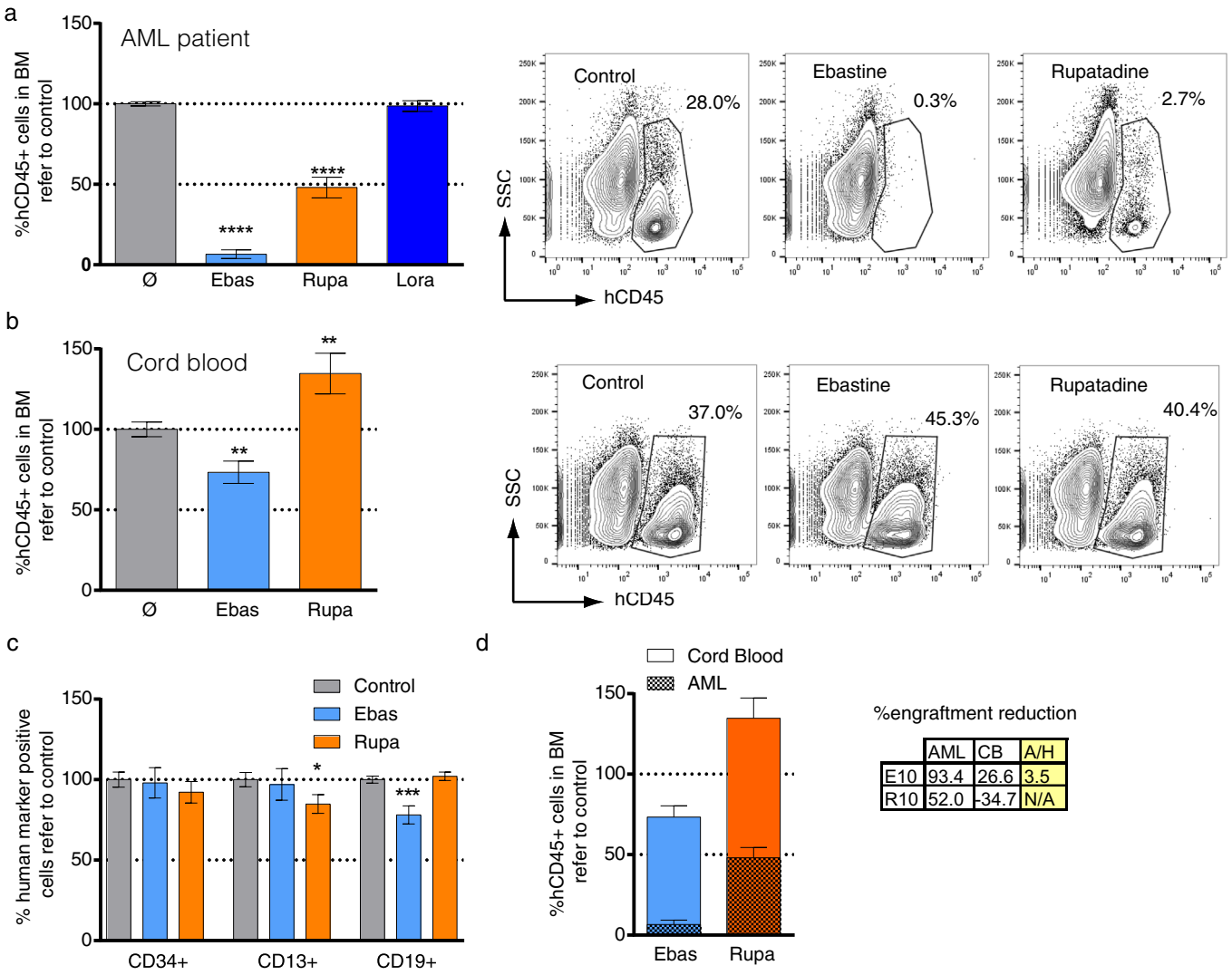

Fig. 3. ANHAs selectively target AML cells *in vivo*. (A).Conditioned NSG mice ($n = 25$) were intravenously transplanted with AML patient samples (AML#2, AML#3 and AML#14) previously treated for 18 h with ebastine 10 μM (Ebas, light blue), rupatadine 10 μM (Rupa, orange) or loratadine 10 μM (Lora, dark blue). After 8 weeks, engraftment was analysed in bone marrow (BM). Frequency of human AML blasts in BM is represented as mean value normalized to vehicle-treated control ± SEM. A representative flow plot from each experimental mouse group is shown. (B). Conditioned NSG mice ($n = 36$) were intravenously transplanted with lineage-depleted cord blood samples (n = 3) previously treated for 18 h with ebastine 10 μM (Ebas, light blue) or rupatadine 10 μM (Rupa, orange). After 8 weeks, engraftment was analysed in bone marrow (BM). Frequency of human blood cells in BM is represented as mean value normalized to vehicle-treated control ± SEM. A representative flow plot from each experimental mouse group is shown. (C). Engrafted cell subpopulations from (B) were analysed according to CD34, CD13 and CD19 positivity to assess changes in the frequency of progenitors, myeloid and B cells respectively. Bars show frequency of each population normalized to vehicle-treated control ± SEM. (D). *In vivo* effects of ANHAs on healthy and AML samples were compared in terms of engrafttment. Data represent engraftment after treatment with ebastine 10 μM (Eb, light blue) or rupatadine 20 μM (Ru, orange). Bars show superimposed mean + SEM of data from Fig. 3A and B. Tables show mean percent reduction of engraftment in AML and cord blood (CB) samples, as well as its fold of change (FC; effect on AML/effect on CB). *p < .05; ** p < .01; *** p < .001; **** p < .0001 (t-tests).

successfully targeted at different levels in acute [57,58] and chronic leukaemias [59]. Indeed, the more primitive leukaemic cell fraction is usually the most sensitive to mitochondria-targeted drugs [58–61]. Sensitivity to mitochondrial damage is thought to be a common property not only of LSCs but also of other cancer stem cell populations [62,63]. Similarly, different effective preclinical therapeutic approaches have been described for lysosome destabilization in leukaemia [40,64–66]. ANHAs damage mitochondria and lysosomes, targeting two fragile organelles in cancer cells. Although an extensive crosstalk between mitochondria and lysosomes is found in cancer cells [67], dual simultaneous targeting may increase efficacy and specificity, constituting a clinical opportunity for selective therapeutic approaches. Due to the inter- and intrapatient heterogeneity and the darwinian nature of leukaemia, combination therapies are likely to provide high specificity in low concentration ranges, reducing toxicity and side effects. ANHAs showed an interesting collaborative effect with currently used cytarabine; thus, sensitizing leukaemic cells to conventional therapy.

The role of antihistamines in cancer has been controversial mainly due to the lack of consistency across different HRH1 inhibitors and the absence of a defined role of its well-described HRH1 molecular target on cancer cells [15]. In haematological neoplasias, several antihistamines have been shown to affect leukaemia cell viability to different extents [17,68–71]. All of them display CAD-associated properties (high logD pH 7.4 and intermedium-low TPSA) compatible to the model proposed. Interestingly, those antihistamines that presented no antileukaemic effect could be predicted by our model [17,68,69,71]. As most CADs, ANHAs are lysosomotropic drugs that induce irreversible damage to lysosomes [40,41]. Recently, certain tropism to mitochondria has been reported for the CAD azidobupramine [47]. Here, a dual

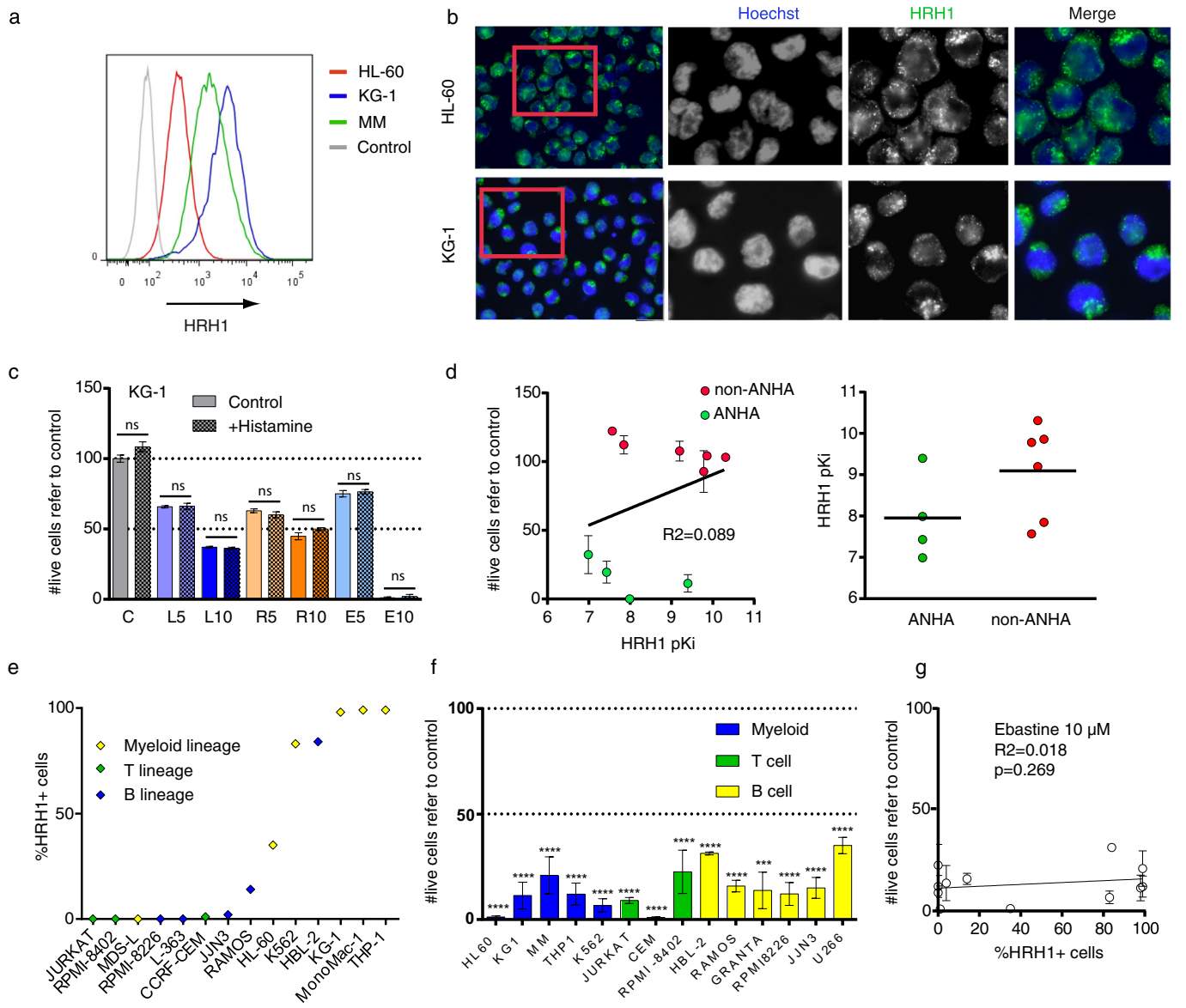

Fig. 4. ANHA's antileukemic effects are independent of HRH1. (A). Representative flow cytometry histograms of HRH1 surface expression on AML cell lines. Grey shadow, control; red line, HL-60; blue line, KG-1; green line, MM. (B). Representative HRH1 surface staining (green) on HL-60 and KG-1 cells by immunofluorescence. Nuclei are stained with Hoechst33342 (blue). (C). KG-1 cells were treated with ANHAs alone or in combination with histamine 200 µM. Viability was measured by flow cytometry (7AAD-, Hoechst+). Bars show mean ± SEM of triplicates from a representative experiment (three independent experiments were performed). (D). 72 h cytotoxicity data from Fig. 1A (antihistamine-treated KG-1 cells) were correlated with the corresponding pKi value for each drug. Left panel includes a regression line and its corresponding R^2. Right panel shows pKis for ANHAs and non-ANHAs. Horizontal lines represent means. (E). Frequency of HRH1 expression on the surface of cell lines from haematological neoplasias, either myeloid (yellow), T (green) or B (blue) lineage, as detected by flow cytometry. (F). Cell lines from different haematological neoplasias were treated for 72 h with ebastine at 10 µM and viability was assessed by flow cytometry. Bars show mean ± SEM of triplicates from 2 independent experiments. (G). 72 h cytotoxicity data from Fig. 4F (Ebastine 10 µM -treated KG-1 cells, Y axis) were correlated with the corresponding %HRH1 expression of each cell line (X axis, data from Fig. 4E). Graphs include regression lines and their corresponding R^2. Right panel shows pKis for ANHAs and non-ANHAs. Error bars represent SEM. *p < .05; ** p < .01; *** p < .001; **** p < .0001 (t-tests).

lysosome/mitochondria targeting is described for ANHA in leukaemic cells, prompting the activation of the lysosome-mediated autophagy and the intrinsic apoptosis, and probably multiplying the selectivity windows given by tumoral alterations (Fig. 7), enabling the development of highly effective therapies with reduced side effects.

Clinical data from the Danish Cancer Register revealed that well-tolerated CAD antihistamines combined with the standard cancer chemotherapy regimen improved survival of solid tumor patients. Remarkably, no clinical benefit was observed when non-CAD antihistamines were assayed [72]. ANHAs have high apparent volumes of distribution [44,72], which facilitates an extensive distribution through all the organs of the body because of their liposolubility and non-ionization. However, low distribution volumes compatible with the therapeutic objective are desirable to avoid side effects and increase effectiveness. Additionally, ANHAs are quickly metabolized in the body and metabolites are not predicted to be active against leukaemia according to the proposed model. Thus, the clinical use of ANHAs will require an extensive pharmacological optimization to

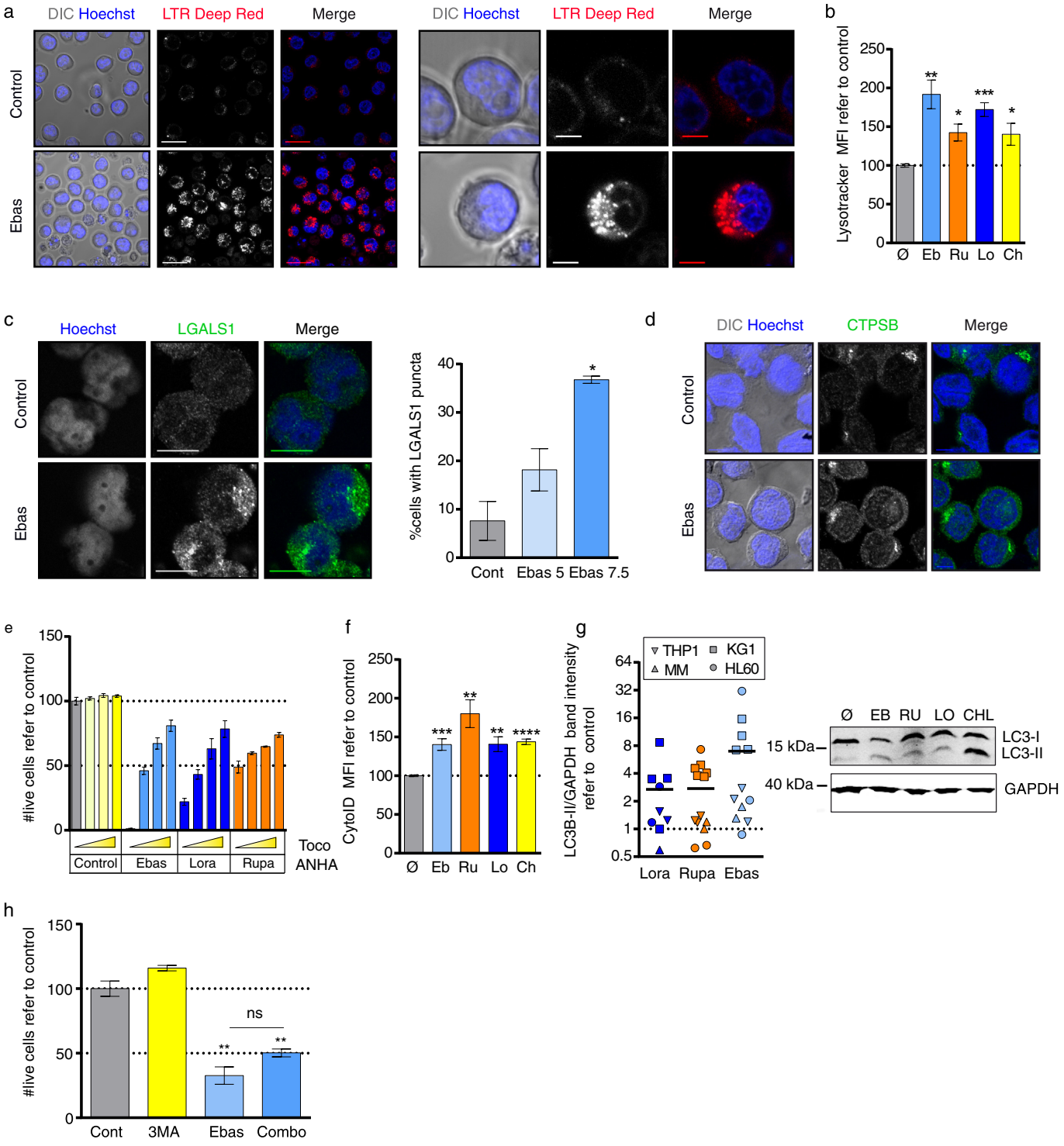

Fig. 5. ANHAs induce an expansion in lysosomal and autophagic compartments. (A). Confocal microscopy images of KG-1 cells treated 18 h with control or ebastine 5 μM, stained with LysoTracker DeepRed 50 nM and Hoechst33342. Left: 630× (scale = 25 μm); right: 1260× (scale = 5 μm). (B). KG-1 cells treated 24 h with control (Ø) ebastine 5 μM (Eb), rupatadine10μM (Ru), loratadine10μM (Lo) or chloroquine20μM (Ch), stained with LysoTracker 50 nM and analysed by cytometry. Bars represent mean ± SEM of triplicates (2 experiments). (C). KG-1 cells were treated 18 h with control or ebastine 5/7.5 μM; galectin-1 (LGALS1, green) distribution was assessed by immunofluorescence. Representative images shown (1260×; scale = 5 μm). Right: frequency of cells with galectin-1 puncta (mean ± SEM, 2 experiments). (D). KG-1 cells were treated 18 h with vehicle control or ebastine 7.5 μM, and cathepsinB (CTSB, green) distribution was assessed by immunofluorescence. Representative images shown (1260×; scale = 5 μm). (E). Viability of KG-1 after 1 h-treatment with α-tocopherol (500, 1000 and 2000 μM) followed by 48 h-treatment with ebastine 10 μM (Ebas), loratadine 10 μM (Lora), or rupatadine 10 μM (Rupa). Bars represent mean ± SEM of triplicates from representative experiment (2 experiments). (F). KG-1 cells treated 48 h with control (Ø) ebastine 5 μM (Eb), rupatadine 10 μM (Ru), loratadine 10 μM (Lo) or chloroquine 20 μM (Ch), stained with CYTO-ID and analysed by flow cytometry. Bars represent mean ± SEM of triplicates (2 experiments). (G). HL-60, KG-1, MonoMac-1 and THP-1 cells were treated 24 h with control (Ø) ebastine 10 μM (Eb), rupatadine 10 μM (Ru), loratadine 10 μM (Lo) or chloroquine 20 μM (Ch). Proteins were extracted and run in a western blot using LC3 and GAPDH antibodies. Representative membranes shown. Data in dot plot; each symbol corresponds to a cell line, each point to a replicate. (H). Viability of KG-1 cells after 48 h-treatment with control (Cont), 3-MA 500 μM, ebastine 7 μM (Ebas) or a combination of both (Combo). Bars show mean ± SEM of triplicates from a representative experiment (2 experiments). *p < .05; ** p < .01; *** p < .001; **** p < .0001 (t-tests).

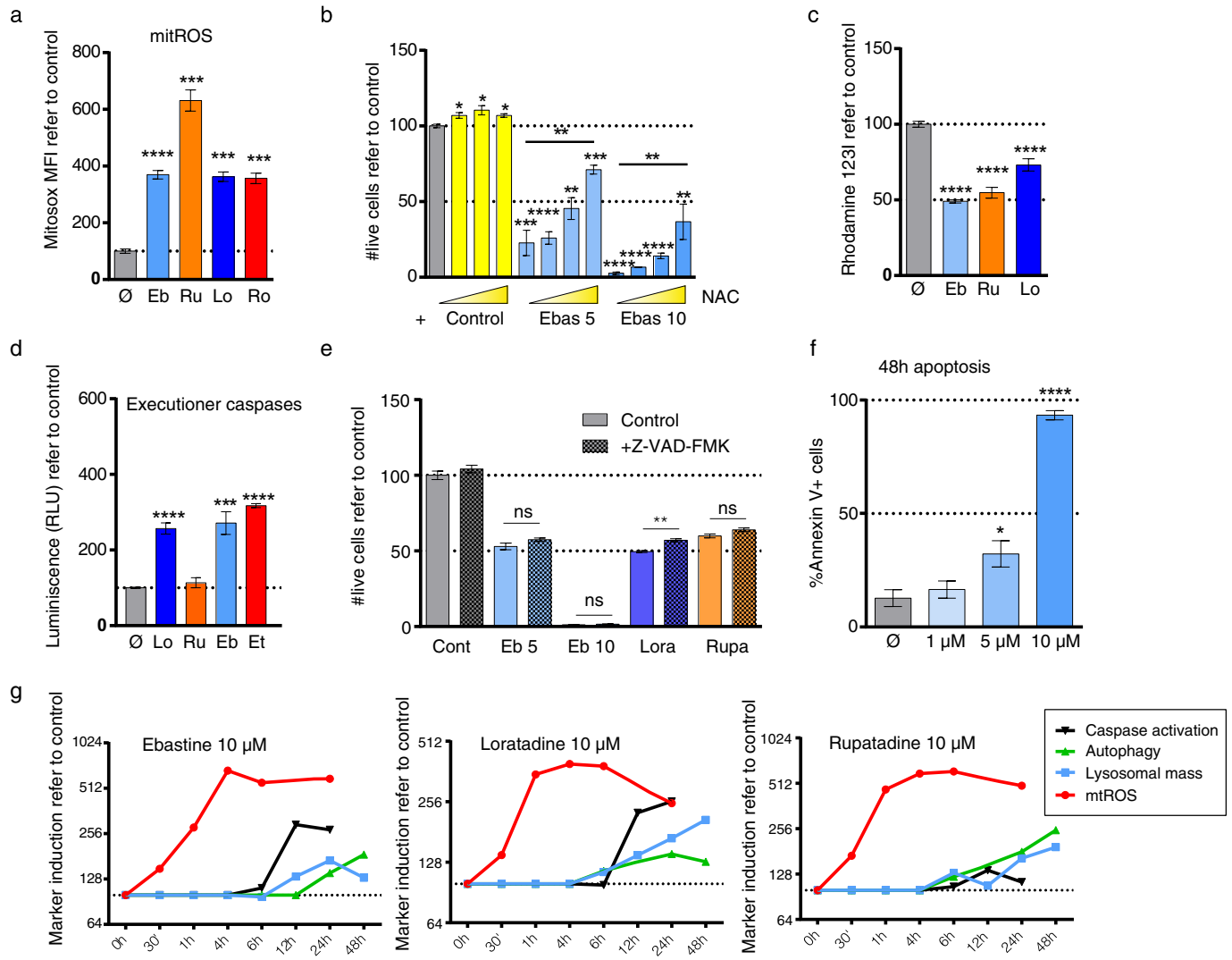

Fig. 6. ANHA-induced cell death partly depends on mitochondrial homeostasis disruption. (A). MitoSOX Red superoxide indicator staining in KG-1 cells were treated 6 h with vehicle control (Ø) ebastine 10 μM (Eb), rupatadine 10 μM (Ru), loratadine 10 μM (Lo) or rotenone 0,1 μM (Ro). Bars show mean ± SEM of triplicates from two independent experiments. (B). THP-1 cells were treated for 48 with increasing concentrations of *N*-acetyl cysteine (NAC; 2, 5 and 10 mM) and ebastine 5 or 10 μM (Ebas). Cell viability was assessed by flow cytometry. Bars represent mean ± SEM of triplicates from a representative experiment (3 independent experiments). (C). KG-1 cells were treated for 18 h with ebastine 7.5 μM (Eb5, Eb10), loratadine 10 μM (Lora) or rupatadine 10 μM (Rupa). After 18 h, cells were stained with rhodamine 123 and analysed by flow cytometry. Bars show mean ± SEM of triplicates from two independent experiments (D). KG-1 cells were treated for 6 or 24 h with vehicle control (grey), loratadine 10 μM (dark blue), rupatadine 10 μM (orange), ebastine 10 μM (light blue) or etoposide 5 μM (red). Caspase activation was analysed using Caspase-Glo ® 3/7 assay. Bars show mean ± SEM of triplicates from two independent experiments (E). KG-1 cells were treated with ebastine 5 or 10 μM (Eb), loratadine 10 μM (Lora) or rupatadine 10 μM (Rupa) in the presence or absence of *Z*-VAD-FMK 50 μM, and viability was assessed after 48 h. Bars show mean ± SEM of triplicates from a representative experiment (out of 3 independent experiments) (F). KG-1 cells were treated with ebastine 1, 5 or 10 μM and frequency of annexin V+ cells was assessed by flow cytometry at 48 h. Bars show mean ± SEM of triplicates from a representative experiment (3 independent experiments) *p < .05; ** p < .01; *** p < .001; **** p < .0001 (t-tests).

improve biodistribution and pharmacokinetics (including metabolism protection). Recently, a new formulation of two commonly used chemotherapeutics has been approved for AML. CPX-351 (Vyxeos, Jazz Pharmaceuticals) is a new liposomal formulation that encapsulates cytarabine and daunorubicin in a fix molar rate. Cytarabine and daunorubicin are rapidly metabolized after administration and become undetectable within the first hour. However, CPX-351-encapsulated cytarabine and daunorubicin administration produce sustained plasma levels of both drugs for several hours, protecting both drugs from metabolism and elimination. Moreover, leukaemic cells exhibit preferential uptake of CPX-351 liposomes when compared with healthy cells [73–75]. Therefore, future clinical development of a liposome-based encapsulated form of ANHA drugs might overcome the high metabolism rate, permitting a sustained presence of non-catabolized ANHA drugs able to widely reach leukaemic cells.

Here, a group of physicochemical properties present in some antihistamines has been defined for specifically passive targeting of leukaemic cells, particularly the most primitive cellular subpopulation of LSCs. The antineoplastic effect is mediated by the concurrent disruption of lysosomal and mitochondrial homeostasis in cancer cells, which are more sensitive than their healthy counterparts. This therapeutic strategy seems to be highly specific and widely safe. However, drug delivery optimization is needed for achievement of the therapeutic dose at the cancer cell localization. Targeting the mitochondrial and lysosomal compartment in leukaemic cells holds great promises in the fight against leukaemia as it provides an alternative pathway to currently

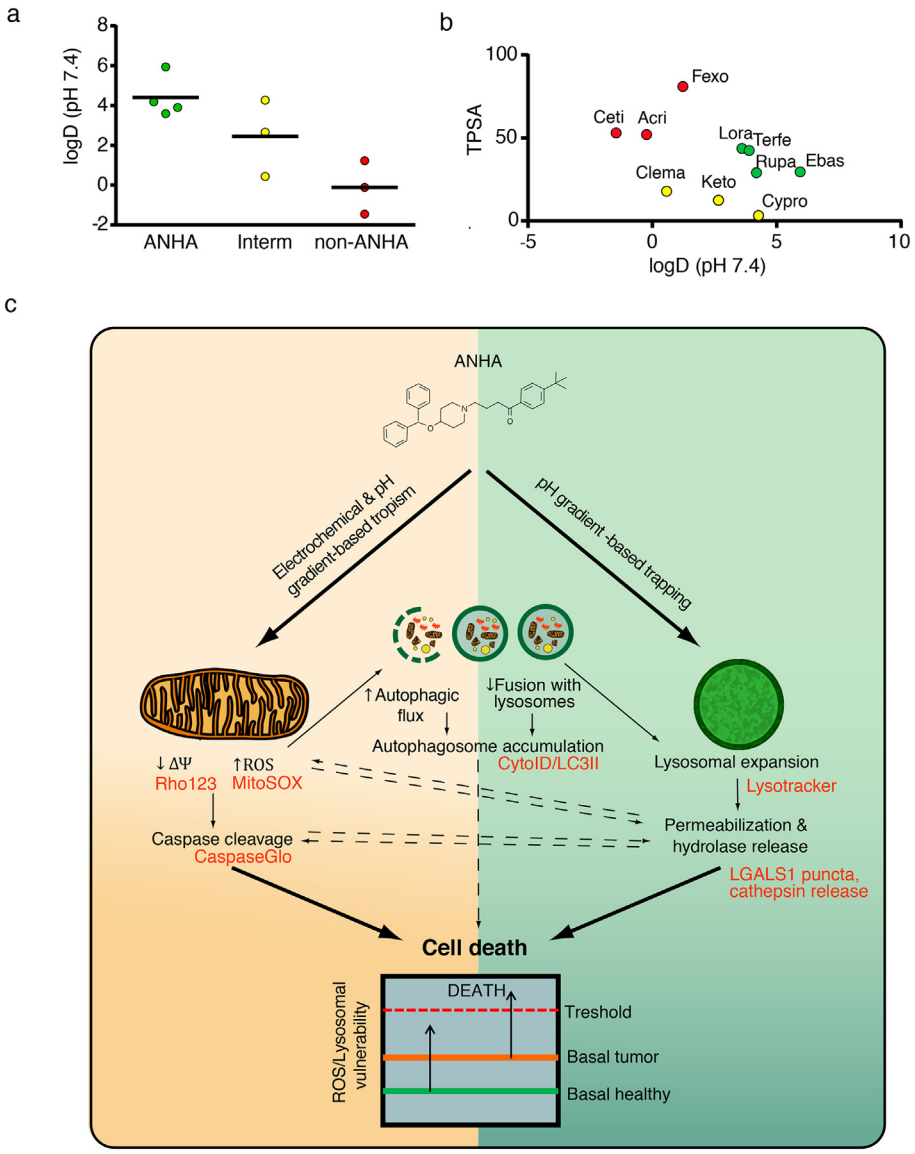

Fig. 7. ANHAs simultaneously target mitochondria and lysosomes (A).KG-1 cells were treated with ebastine 10 μM, loratadine 10 μM or rupatadine 10 μM and different parameters were analysed at the indicated times; caspase activation (caspaseGLO), autophagy (CYTO-ID), lysosomal volume (LysoTracker) and mitochondrial ROS (MitoSOX). Each point represents the mean of triplicates from two independent experiments. (B). Calculated $logD_{7,4}$ values obtained from ChEMBL (ACDLabs calculations) were plotted for each functional antihistamine group. Each point represents an antihistamine (C). Antihistamines were plotted according to their calculated $logD_{7,4}$ and their calculated topological polar surface area (TPSA, drugbank.ca). ANHAs are represented in green, non-ANHAs in red, and intermediate antihistamines in yellow. (D). Model depicting the hypothesized antileukaemic mechanism of action of antihistamines.

used chemotherapy that engages alternative cell death programs to which leukaemic cells are sensitive.

Author contributions

JMCM, designed and performed experiments, analysed the data, and wrote the manuscript. ABM and JMC, performed experiments and analysed the data. MAT, FG and JE, provided patient samples and clinical data. LCC, assisted with experimental work. RMR, designed the project, analysed the data, interpreted results and wrote the manuscript. All authors discussed the results and commented on the manuscript.

Declaration of Competing Interest

Dr. Muñoz Risueño reports grants from Ramón y Cajal program, grants from Fundación Mutua Madrileña, grants from CaixaImpulse, grants from MINECO, grants from Josep Carreras International Leukaemia Research Foundation, grants from Obra Social La Caixa-Fundació Bancària La Caixa, grants from CERCA Programme, during the conduct of the study; and RMR is a shareholder of Leukos Biotech.

Acknowledgements

We would like to thank all members of the Risueño Laboratory for helpful discussions and technical support, and Martí Duran-Ferrer (IDIBAPS, Barcelona, Spain) for assistance with bioinformatics analysis. We would like to acknowledge the technical help of the Advanced Optical Microscopy Unit (Scientific and Technological Centers of the University of Barcelona-CCiTUB, Campus Medicine Clínic, Barcelona, Spain). RMR is supported by Ramón y Cajal program of the Spanish Ministry of Economy (RYC-2011-07998 and IEDI-2016-00740), and JMCM is supported by Fundación Mutua Madrileña. This work was funded by the Fundación Mutua Madrileña (RMR), CaixaImpulse CI16-00003 (RMR), SAF2015-66721-P from MINECO (RMR), the Josep Carreras International Leukaemia Foundation (RMR), l'Obra Social "La Caixa"-Fundació Bancària "La Caixa" (RMR), and CERCA Programme/

Generalitat de Catalunya (IJC). RMR had full access to all the data in the study and had final responsibility for the decision to submit for publication. Funding sources provided economical support to the experimental work presented here.

Appendix A. Supplementary data

Supplementary data to this article can be found online at https://doi.org/10.1016/j.ebiom.2019.08.021.

References

[1] Moarii M, Papaemmanuil E. Classification and risk assessment in AML: integrating cytogenetics and molecular profiling. Hematol Am Soc Hematol Educ Progr 2017; 2017:37–44. https://doi.org/10.1182/asheducation-2017.1.37.

[2] Ding L, Ley TJ, Larson DE, Miller CA, Koboldt DC, Welch JS, et al. Clonal evolution in relapsed acute myeloid leukaemia revealed by whole-genome sequencing. Nature 2012;481:506–10. https://doi.org/10.1038/nature10738.

[3] Ley TJ, Ding L, Walter MJ, McLellan MD, Lamprecht T, Larson DE, et al. *DNMT3A* mutations in acute myeloid leukemia. N Engl J Med 2010;363:2424–33. https://doi.org/10.1056/NEJMoa1005143.

[4] Mardis ER, Ding L, Dooling DJ, Larson DE, McLellan MD, Chen K, et al. Recurring mutations found by sequencing an acute myeloid leukemia genome. N Engl J Med 2009; 361:1058–66. https://doi.org/10.1056/NEJMoa0903840.

[5] Welch JS, Ley TJ, Link DC, Miller CA, Larson DE, Koboldt DC, et al. The origin and evolution of mutations in acute myeloid leukemia. Cell 2012;150:264–78. https://doi.org/10.1016/j.cell.2012.06.023.

[6] Walter MJ, Shen D, Ding L, Shao J, Koboldt DC, Chen K, et al. Clonal architecture of secondary acute myeloid leukemia. N Engl J Med 2012;366:1090–8. https://doi.org/10.1056/NEJMoa1106968.

[7] Papaemmanuil E, Gerstung M, Bullinger L, Gaidzik VI, Paschka P, Roberts ND, et al. Genomic classification and prognosis in acute myeloid leukemia. N Engl J Med 2016;374:2209–21. https://doi.org/10.1056/NEJMoa1516192.

[8] Look AT. Oncogenic transcription factors in the human acute leukemias. Science 1997;278:1059–64. https://doi.org/10.1126/science.278.5340.1059 (80-).

[9] Buechele C, Breese EH, Schneidawind D, Lin CH, Jeong J, Duque-Afonso J, et al. MLL leukemia induction by genome editing of human CD34+ hematopoietic cells. Blood 2015;126:1683–94. https://doi.org/10.1182/blood-2015-05-646398.

[10] Wei J, Wunderlich M, Fox C, Alvarez S, Cigudosa JC, Wilhelm JS, et al. Microenvironment determines lineage fate in a human model of MLL-AF9 leukemia. Cancer Cell 2008;13:483–95. https://doi.org/10.1016/j.ccr.2008.04.020.

[11] Barabé F, Gil L, Celton M, Bergeron A, Lamontagne V, Roques, et al.. Modeling human MLL-AF9 translocated acute myeloid leukemia from single donors reveals RET as a potential therapeutic target. Leukemia 2017;31:1166–76. https://doi.org/10.1038/leu.2016.302.

[12] Krivtsov AV, Armstrong SA. MLL translocations, histone modifications and leukaemia stem-cell development. Nat Rev Cancer 2007;7:823–33. https://doi.org/10.1038/nrc2253.

[13] Biondi A, Cimino G, Pieters R, Pui CH. Biological and therapeutic aspects of infant leukemia. Blood 2000;96:24–33.

[14] Kahlson G, Rosengren E. New approaches to the physiology of histamine. Physiol Rev 1968;48:155–96. https://doi.org/10.1152/physrev.1968.48.1.155.

[15] Faustino-Rocha AI, Ferreira R, Gama A, Oliveira PA, Ginja M. Antihistamines as promising drugs in cancer therapy. Life Sci 2017;172:27–41. https://doi.org/10.1016/j.lfs.2016.12.008.

[16] Cianchi F, Cristina Vinci M, Masini E. Histamine in cancer: the dual faces of the coin. Cancer Biol Ther 2008;7:36–7. https://doi.org/10.4161/cbt.7.1.5706.

[17] Laverdière I, Boileau M, Neumann AL, Frison H, Mitchell A, Ng SWK, et al. Leukemic stem cell signatures identify novel therapeutics targeting acute myeloid leukemia. Blood Cancer J 2018;8:52. https://doi.org/10.1038/s41408-018-0087-2.

[18] Ellegaard A-M, Dehlendorff C, Vind AC, Anand A, Cederkvist L, Petersen NHT, et al. Repurposing cationic amphiphilic antihistamines for Cancer treatment. EBioMedicine 2016;9:130–9. https://doi.org/10.1016/j.ebiom.2016.06.013.

[19] Wang W-T, Chen Y-H, Hsu J-L, Leu W-J, Yu C-C, Chan S-H, et al. Terfenadine induces anti-proliferative and apoptotic activities in human hormone-refractory prostate cancer through histamine receptor-independent Mcl-1 cleavage and Bak up-regulation. Naunyn Schmiedebergs Arch Pharmacol 2014;387:33–45. https://doi.org/10.1007/s00210-013-0912-x.

[20] Aichberger KJ. Identification of mcl-1 as a BCR/ABL-dependent target in chronic myeloid leukemia (CML): evidence for cooperative antileukemic effects of imatinib and mcl-1 antisense oligonucleotides. Blood 2005;105:3303–11. https://doi.org/10.1182/blood-2004-02-0749.

[21] Liu J-D, Wang Y-J, Chen C-H, Yu C-F, Chen L-C, Lin J-K, et al. Molecular mechanisms of G 0 /G 1 cell-cycle arrest and apoptosis induced by Terfenadine in human cancer cells. Mol Carcinog 2003. https://doi.org/10.1002/mc.10118.

[22] Soule BP, Simone NL, DeGraff WG, Choudhuri R, Cook JA, Mitchell JB. Loratadine dysregulates cell cycle progression and enhances the effect of radiation in human tumor cell lines. Radiat Oncol 2010;5. https://doi.org/10.1186/1748-717X-5-8.

[23] Brandes LJ, Warrington RC, Arron RJ, Bogdanovic RP, Fang W, Queen GM, et al. Enhanced Cancer growth in mice administered daily human-equivalent doses of some H1-antihistamines: predictive in vitro correlates. JNCI J Natl Cancer Inst 1994;86:770–5. https://doi.org/10.1093/jnci/86.10.770.

[24] Jangi SM, Díaz-Pérez JL, Ochoa-Lizarralde B, Martín-Ruiz I, Asumendi A, Pérez-Yarza G, et al. H1 histamine receptor antagonists induce genotoxic and caspase-2-dependent apoptosis in human melanoma cells. Carcinogenesis 2006;27:1787–96. https://doi.org/10.1093/carcin/bgl021.

[25] Schindelin J, Arganda-Carreras I, Frise E, Kaynig V, Longair M, Pietzsch T, et al. Fiji: an open-source platform for biological-image analysis. Nat Methods 2012;9:676–82. https://doi.org/10.1038/nmeth.2019.

[26] Krivtsov AV, Twomey D, Feng Z, Stubbs MC, Wang Y, Faber J, et al. Transformation from committed progenitor to leukaemia stem cell initiated by MLL-AF9. Nature 2006;442:818–22. https://doi.org/10.1038/nature04980.

[27] Abdul-Nabi AM, Yassin ER, Varghese N, Deshmukh H, Yaseen NR. In vitro transformation of primary human CD34+ cells by AML fusion oncogenes: early gene expression profiling reveals possible drug target in AML. PLoS One 2010;5:e12464. https://doi.org/10.1371/journal.pone.0012464.

[28] Lamb J, Crawford ED, Peck D, Modell JW, Blat IC, Wrobel MJ, et al. The connectivity map: using gene-expression signatures to connect small molecules, genes, and disease. Science 2006;313:1929–35. https://doi.org/10.1126/science.1132939.

[29] Meads MB, Hazlehurst LA, Dalton WS. The bone marrow microenvironment as a tumor sanctuary and contributor to drug resistance. Clin Cancer Res 2008;14: 2519–26. https://doi.org/10.1158/1078-0432.CCR-07-2223.

[30] Schulz M, Schmoldt A. Therapeutic and toxic blood concentrations of more than 800 drugs and other xenobiotics. Pharmazie 2003;58:447–74.

[31] Paakkari I. Cardiotoxicity of new antihistamines and cisapride. Toxicol Lett 2002; 127:279–84. https://doi.org/10.1016/S0378-4274(01)00510-0.

[32] Zhang M-Q, Walczynski K, Ter Laak AM, Timmerman H. Optically active analogues of ebastine: synthesis and effect of chirality on their antihistaminic and antimuscarinic activity. Chirality 1994;6:631–41. https://doi.org/10.1002/chir.530060806.

[33] Orzechowski RF, Currie DS, Valancius CA. Comparative anticholinergic activities of 10 histamine H1 receptor antagonists in two functional models. Eur J Pharmacol 2005;506:257–64. https://doi.org/10.1016/j.ejphar.2004.11.006.

[34] Simons FER. Advances in H 1 -antihistamines. N Engl J Med 2004;351:2203–17. https://doi.org/10.1056/NEJMra033121.

[35] Ko CM, Ducic I, Fan J, Shuba YM, Morad M. Suppression of mammalian K+ channel family by ebastine. J Pharmacol Exp Ther 1997;281:233–44.

[36] Aslanian R, Piwinski JJ, Zhu X, Priestley T, Sorota S, Du X-Y, et al. Structural determinants for histamine H1 affinity, hERG affinity and QTc prolongation in a series of terfenadine analogs. Bioorg Med Chem Lett 2009;19:5043–7. https://doi.org/10.1016/j.bmcl.2009.07.047.

[37] Leurs R, Church MK, Taglialatela M. H1-antihistamines: inverse agonism, anti-inflammatory actions and cardiac effects. Clin Exp Allergy Exp Allergy 2002;32: 489–98. https://doi.org/10.1046/j.0954-7894.2002.01314.x.

[38] Kodavanti UP, Mehendale HM. Cationic amphiphilic drugs and phospholipid storage disorder. Pharmacol Rev 1990;42:327–54.

[39] Smith D, Artursson P, Avdeef A, Di L, Ecker GF, Faller B, et al. Passive Lipoidal diffusion and carrier-mediated cell uptake are both important mechanisms of membrane permeation in drug disposition. Mol Pharm 2014;11:1727–38. https://doi.org/10.1021/mp400713v.

[40] Sukhai MA, Prabha S, Hurren R, Rutledge AC, Lee AY, Sriskanthadevan S, et al. Lysosomal disruption preferentially targets acute myeloid leukemia cells and progenitors. J Clin Invest 2013;123. https://doi.org/10.1172/JCI64180.

[41] Petersen NHT, Olsen OD, Groth-Pedersen L, Ellegaard A-M, Bilgin M, Redmer S, et al. Transformation-associated changes in sphingolipid metabolism sensitize cells to lysosomal cell death induced by inhibitors of acid sphingomyelinase. Cancer Cell 2013;24:379–93. https://doi.org/10.1016/j.ccr.2013.08.003.

[42] Galluzzi L, Vitale I, Aaronson SA, Abrams JM, Adam D, Agostinis P, et al. Molecular mechanisms of cell death: recommendations of the Nomenclature Committee on Cell Death 2018. Cell Death Differ 2018;25:486. https://doi.org/10.1038/s41418-017-0012-4 2018 253.

[43] Aits S, Jäättelä M, Nylandsted J. Methods for the quantification of lysosomal membrane permeabilization: a hallmark of lysosomal cell death. Methods Cell Biol 2015:261–85. https://doi.org/10.1016/bs.mcb.2014.10.032.

[44] Marenchino M, Alpstäg-Wöhrle AL, Christen B, Wunderli-Allenspach H, Krämer SD. α-Tocopherol influences the lipid membrane affinity of desipramine in a pH-dependent manner. Eur J Pharm Sci 2004;21:313–21. https://doi.org/10.1016/j.ejps.2003.10.022.

[45] Quinn PJ. Is the distribution of -tocopherol in membranes consistent with its putative functions? Biochem 2004;69:58–66. https://doi.org/10.1023/B:BIRY.0000016352.88061.02.

[46] Klionsky DJ, Abdelmohsen K, Abe A, Abedin MJ, Abeliovich H, Acevedo Arozena A, et al. Guidelines for the use and interpretation of assays for monitoring autophagy (3rd edition). Autophagy 2016;12:1–222. https://doi.org/10.1080/15548627.2015.1100356.

[47] Vater M, Möckl L, Gormanns V, Schultz Fademrecht C, Mallmann AM, Ziegart-Sadowska K, et al. New insights into the intracellular distribution pattern of cationic amphiphilic drugs. Sci Rep 2017;7:44277. https://doi.org/10.1038/srep44277.

[48] KÅGEDAL K, ZHAO M, SVENSSON I, BRUNK UT. Sphingosine-induced apoptosis is dependent on lysosomal proteases. Biochem J 2001;359:335–43. https://doi.org/10.1042/bj3590335.

[49] Bernard D, Gebbia M, Prabha S, Gronda M, MacLean N, Wang X, et al. Select microtubule inhibitors increase lysosome acidity and promote lysosomal disruption in acute myeloid leukemia (AML) cells. Apoptosis 2015;20:948–59. https://doi.org/10.1007/s10495-015-1123-3.

[50] Boultwood J, Fidler C, Mills KI, Frodsham PM, Kusec R, Gaiger A, et al. Amplification of mitochondrial DNA in acute myeloid leukaemia. Br J Haematol 1996;95:426–31. https://doi.org/10.1046/j.1365-2141.1996.d01-1922.x.

[51] Sallmyr A, Fan J, Datta K, Kim K-T, Grosu D, Shapiro P, et al. Internal tandem duplication of FLT3 (FLT3/ITD) induces increased ROS production, DNA damage, and

misrepair: implications for poor prognosis in AML. Blood 2008;111:3173–82. https://doi.org/10.1182/blood-2007-05-092510.
[52] Sriskanthadevan S, Jeyaraju DV, Chung TE, Prabha S, Xu W, Skrtic M, et al. AML cells have low spare reserve capacity in their respiratory chain that renders them susceptible to oxidative metabolic stress. Blood 2015;125:2120–30. https://doi.org/10.1182/blood-2014-08-594408.
[53] Molina JR, Sun Y, Protopopova M, Gera S, Bandi M, Bristow C, et al. An inhibitor of oxidative phosphorylation exploits cancer vulnerability. Nat Med 2018;24:1036–46. https://doi.org/10.1038/s41591-018-0052-4.
[54] Chen W-L, Wang J-H, Zhao A-H, Xu X, Wang Y-H, Chen T-L, et al. A distinct glucose metabolism signature of acute myeloid leukemia with prognostic value. Blood 2014;124:1645–54. https://doi.org/10.1182/blood-2014-02-554204.
[55] Dielschneider RF, Henson ES, Gibson SB. Lysosomes as oxidative targets for Cancer therapy. Oxid Med Cell Longev 2017;2017:1–8. https://doi.org/10.1155/2017/3749157.
[56] Aits S, Jaattela M. Lysosomal cell death at a glance. J Cell Sci 2013;126:1905–12. https://doi.org/10.1242/jcs.091181.
[57] Fu X, Liu W, Huang Q, Wang Y, Li H, Xiong Y. Targeting mitochondrial respiration selectively sensitizes pediatric acute lymphoblastic leukemia cell lines and patient samples to standard chemotherapy. Am J Cancer Res 2017;7:2395–405.
[58] Lagadinou ED, Sach A, Callahan K, Rossi RM, Neering SJ, Minhajuddin M, et al. BCL-2 inhibition targets oxidative phosphorylation and selectively eradicates quiescent human leukemia stem cells. Cell Stem Cell 2013;12:329–41. https://doi.org/10.1016/j.stem.2012.12.013.
[59] Kuntz EM, Baquero P, Michie AM, Dunn K, Tardito S, Holyoake TL, et al. Targeting mitochondrial oxidative phosphorylation eradicates therapy-resistant chronic myeloid leukemia stem cells. Nat Med 2017;23:1234–40. https://doi.org/10.1038/nm.4399.
[60] Pei S, Minhajuddin M, Adane B, Khan N, Stevens BM, Mack SC, et al. AMPK/FIS1-Mediated Mitophagy Is Required for Self-Renewal of Human AML Stem Cells. Cell Stem Cell 2018;23. https://doi.org/10.1016/j.stem.2018.05.021 (86–100.e6).
[61] Škrtić M, Sriskanthadevan S, Jhas B, Gebbia M, Wang X, Wang Z, et al. Inhibition of mitochondrial translation as a therapeutic strategy for human acute myeloid leukemia. Cancer Cell 2011;20:674–88. https://doi.org/10.1016/j.ccr.2011.10.015.
[62] Roesch A, Vultur A, Bogeski I, Wang H, Zimmermann KM, Speicher D, et al. Overcoming intrinsic multidrug resistance in melanoma by blocking the mitochondrial respiratory chain of slow-cycling JARID1B high cells. Cancer Cell 2013;23. https://doi.org/10.1016/j.ccr.2013.05.003.
[63] Viale A, Pettazzoni P, Lyssiotis CA, Ying H, Sánchez N, Marchesini M, et al. Oncogene ablation-resistant pancreatic cancer cells depend on mitochondrial function. Nature 2014;514:628–32. https://doi.org/10.1038/nature13611.
[64] Sukhai MA, Spagnuolo PA, Weir S, Kasper J, Patton L, Schimmer AD. New sources of drugs for hematologic malignancies. Blood 2011;117:6747–55. https://doi.org/10.1182/blood-2011-02-315283.
[65] Dielschneider R, Eisenstat H, Johnston JB, Gibson SB. Lysosome membrane Permeabilization causes cell death in primary chronic lymphocytic leukemia cells. Blood 2014;124:930.
[66] Puissant A, Dufies M, Raynaud S, Cassuto J-P, Auberger P. Targeting lysosomes to eradicate imatinib-resistant chronic myelogenous leukemia cells. Leukemia 2010;24:1099–101. https://doi.org/10.1038/leu.2010.55.
[67] Kirkegaard T, Jäättelä M. Lysosomal involvement in cell death and cancer. Biochim Biophys Acta - Mol Cell Res 1793;2009:746–54. https://doi.org/10.1016/j.bbamcr.2008.09.008.
[68] Chanas-LaRue AP, Johnston JB, Gibson SB. Abstract 3976: Antihistamines as synergists with targeted therapies in chronic lymphocytic leukemia. Cancer Res 2018;78(13 Suppl):3976. https://doi.org/10.1158/1538-7445.AM2018-3976 American Association for Cancer Research.
[69] Mao X. Liang S -b., Hurren R, Gronda M, chow S, Xu GW, et al. Cyproheptadine displays preclinical activity in myeloma and leukemia. Blood 2008;112:760–9. https://doi.org/10.1182/blood-2008-02-142687.
[70] Jangi S-M, Ruiz-Larrea MB, Nicolau-Galmes F, Andollo N, Arroyo-Berdugo Y, Ortega-Martinez I, et al. Terfenadine-induced apoptosis in human melanoma cells is mediated through Ca2+ homeostasis modulation and tyrosine kinase activity, independently of H1 histamine receptors. Carcinogenesis 2007;29:500–9. https://doi.org/10.1093/carcin/bgm292.
[71] Aichberger KJ, Mayerhofer M, Vales A, Krauth MT, Gleixner KV, Bilban M, et al. The CML-related oncoprotein BCR/ABL induces expression of histidine decarboxylase (HDC) and the synthesis of histamine in leukemic cells. Blood 2006;108:3538–47. https://doi.org/10.1182/blood-2005-12-028456.
[72] Ellegaard AM, Dehlendorff C, Vind AC, Anand A, Cederkvist L, Petersen NHT, et al. Repurposing cationic amphiphilic antihistamines for cancer treatment. EBioMedicine 2016;9:130–9. https://doi.org/10.1016/j.ebiom.2016.06.013.
[73] Tardi P, Johnstone S, Harasym N, Xie S, Harasym T, Zisman N, et al. In vivo maintenance of synergistic cytarabine:daunorubicin ratios greatly enhances therapeutic efficacy. Leuk Res 2009;33:129–39. https://doi.org/10.1016/j.leukres.2008.06.028.
[74] Feldman EJ, Kolitz JE, Trang JM, Liboiron BD, Swenson CE, Chiarella MT, et al. Pharmacokinetics of CPX-351; a nano-scale liposomal fixed molar ratio formulation of cytarabine:daunorubicin, in patients with advanced leukemia. Leuk Res 2012;36:1283–9. https://doi.org/10.1016/j.leukres.2012.07.006.
[75] Luppi M, Fabbiano F, Visani G, Martinelli G, Venditti A. Novel agents for acute myeloid leukemia. Cancers (Basel) 2018;10:429. https://doi.org/10.3390/cancers10110429.